Journal of Power Sources 434 (2019) 226750

Contents lists available at ScienceDirect

Journal of Power Sources

journal homepage: www.elsevier.com/locate/jpowsour

Monoclinic $Fe_2(SO_4)_3$: A new Fe-based cathode material with superior electrochemical performances for Na-ion batteries

Hyunyoung Park [a], Jung-Keun Yoo [b], Wonseok Ko [a], Yongseok Lee [a], Inchul Park [c], Seung-Taek Myung [a,**], Jongsoon Kim [a,*]

[a] Department of Nanotechnology and Advanced Materials Engineering, Sejong University, Seoul, 05006, Republic of Korea
[b] Carbon Composites Department, Composites Research Division, Korea Institute of Materials Science (KIMS), 797 Changwondae-ro, Changwon, Republic of Korea
[c] Materials Research Laboratory, Research Institute of Industrial Science & Technology, 67 Cheongam-ro, Pohang, Republic of Korea

HIGHLIGHTS

- First-principles calculation for theoretical approach of monoclinic $Fe_2(SO_4)_3$.
- ~120 mAh g^{-1} at C/10, corresponding to ~1.8 mol of Na intercalation.
- Capacity retention of ~78% of the initial capacity over 1000 cycles at 1C.

GRAPHICAL ABSTRACT

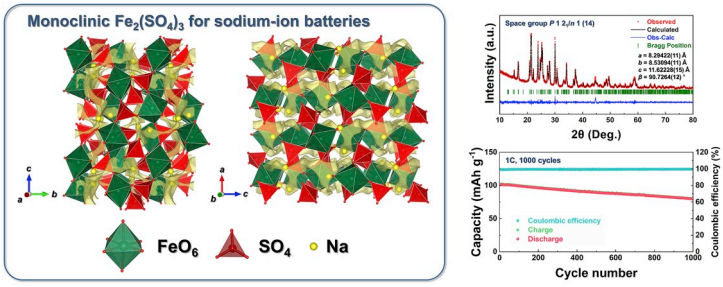

ARTICLE INFO

Keywords:
Cathode
Sodium
Battery
Iron sulfate
First-principles calculation

ABSTRACT

We report monoclinic $Fe_2(SO_4)_3$ as a novel high-voltage cathode material of Na-ion batteries. The detailed structural information of monoclinic $Fe_2(SO_4)_3$ are verified through Rietveld refinement and bond-valance sum energy mapping with X-ray diffraction analyses. Monoclinic $Fe_2(SO_4)_3$ delivers a large specific capacity of ~120 mAh g^{-1} corresponding to ~1.8 mol Na intercalation into the structure and it exhibits the average operation voltage of ~3.25 V (*vs.* Na^+/Na). Even at 5C, monoclinic $Fe_2(SO_4)_3$ exhibits retention of ~76% of the capacity measured at C/10, indicating its outstanding power capability. Moreover, monoclinic $Fe_2(SO_4)_3$ maintains up to ~78% of the initial capacity at 1C over 1000 cycles, with a high Coulombic efficiency of ~99%. This finding demonstrates the excellent cyclability of monoclinic $Fe_2(SO_4)_3$, which results from the small volume change (~1%) during the Na de/intercalation process.

1. Introduction

The application of rechargeable batteries is widening from small electronic devices, such as mobile phones and laptops, to large-scale energy sources, such as energy storage systems (ESSs) for electric vehicles (EVs), with the demand for rechargeable batteries dramatically growing worldwide [1–5]. Among the various types of rechargeable batteries, Li-ion batteries (LIBs) have received substantial attention

* Corresponding author.
** Corresponding author.
E-mail addresses: smyung@sejong.ac.kr (S.-T. Myung), jongsoonkim@sejong.ac.kr (J. Kim).

https://doi.org/10.1016/j.jpowsour.2019.226750
Received 1 May 2019; Received in revised form 3 June 2019; Accepted 10 June 2019
Available online 15 June 2019
0378-7753/

because of their high energy density and stable cycle life [6–9]. Nevertheless, recent fluctuations in the price of lithium have resulted in high production costs for LIBs; thus, low-cost alternatives to LIBs are needed to realize the widespread application of grid-scale EESs [10,11]. Recently, Na-ion batteries (NIBs) have been considered one of the most promising alternatives to LIBs because of the abundance of Na resources and the similar reaction chemistries of NIBs and LIBs [12–17]. However, the higher standard electrode potential of Na^+/Na (−2.71 V *vs.* standard hydrogen electrode (*SHE*)) versus Li^+/Li (−3.01 V *vs. SHE*) results in an intrinsically lower energy density, necessitating the development of high-voltage cathode materials to enable NIBs to compete with LIBs. The strategy to increase the redox potential of cathode materials is to utilize the inductive effect by anion groups with high electronegativity. When transition metal (TM) ions share oxygen ions with the anion groups, the covalent bonds between the TM and oxygen ions may be weakened by the electron-withdrawing property of the anion groups. As a result, the gap between the bonding and anti-bonding orbitals is reduced, leading to upshifting of the redox potential of the electrode materials. Sulfate ($(SO_4)^{2-}$)-based polyanions have been shown to increase the operation voltage compared to other polyanions, such as phosphate, silicate, *etc* [18–31]. In particular, in case of $Fe_2(SO_4)_3$ composition, there are two-type crystal structures, such as rhombohedral and monoclinic structures. Recently, it was reported that Na ions can be intercalated into the rhombohedral $Fe_2(SO_4)_3$ with the average voltage of ~3.2 V (*vs.* Na^+/Na) [29]. On the other hand, unlike rhombohedral $Fe_2(SO_4)_3$, the detailed studies on monoclinic $Fe_2(SO_4)_3$ under the NIB system has not been reported.

Herein, we demonstrated the electrochemical performances and the reaction mechanism of monoclinic $Fe_2(SO_4)_3$ (M-$Fe_2(SO_4)_3$) as a cathode for NIBs using combined studies of various experiments and first-principles calculation. With the operation voltage of ~3.25 V (*vs.* Na^+/Na), it exhibited a large discharge capacity of ~120.3 mAh g^{-1} at C/10 (1C = ~133 mA g^{-1}), corresponding to reversible de/intercalation of ~1.8 mol Na ions per formula unit in the structure. At 5C, up to ~76% of the discharge capacity of M-$Fe_2(SO_4)_3$ at C/10 is maintained, demonstrating the excellent power capability of M-$Fe_2(SO_4)_3$. Furthermore, M-$Fe_2(SO_4)_3$ exhibited unexpectedly outstanding cyclability over 1000 cycles with ~78% retention of its initial capacity at 1C. Theoretical studies using first-principles calculations provided the additional insight to understand the outstanding electrochemical performance of M-$Fe_2(SO_4)_3$ under NIB system.

2. Experimental section

2.1. Synthesis of monoclinic $Fe_2(SO_4)_3$

$FeSO_4{\cdot}7H_2O$ (98.0–102.0%, Samchun Chemicals) was mixed with H_2SO_4 (98%, Daejung Chemicals & Metals), and the precursor was synthesized at 100 °C using H_2O_2 (98%, Daejung Chemicals & Metals) as an oxidizing agent [18,22,24]. The pink-color precursor was filtered sequentially with H_2SO_4 and anhydrous ethanol (99.9%, Daejung Chemicals & Metals) and heated at 380 °C to remove residual moisture and H_2SO_4.

2.2. Materials characterization

M-$Fe_2(SO_4)_3$ was analyzed using XRD (Malvern Panalytical Empyrean) using Cu Kα radiation (λ = 1.54178 Å). The step size is 0.13°, and the 2θ range of 10°–80° was examined. Rietveld refinement of the XRD data was performed using Fullprof software. The morphology and particle size of M-$Fe_2(SO_4)_3$ were determined using SEM (HITACHI SU-8010) and field-emission TEM (JEOL JEM-F200). Fe K-edge X-ray absorption spectra (XAS) were obtained at the 8C beamline at Pohang Accelerator Laboratory.

2.3. Electrochemical characterization

Pristine M-$Fe_2(SO_4)_3$ and Super P were homogenously mixed using the planetary ball-milling (Fritsch Pulverisette) at a weight ratio of 8 : 2, to enhance the electrical conductivity. The jar was sealed in an Ar glove box and ball-milled at 200 rpm for 12 h. Then, we fabricated the M-$Fe_2(SO_4)_3$ electrode. Total composition of the electrode was adjusted to 70 wt % of the active material, 20 wt % super P, and 10 wt % poly (vinylidene fluoride) (PVdF). A slurry of the mixture was applied to Al foil using a doctor blade. The electrode was dried at 80 °C for 12 h to evaporate the NMP. The mass loading of electrode is ~2 mg cm^{-2}.

CR2032-type coin cells were prepared using a M-$Fe_2(SO_4)_3$ electrode, the reference/counter electrode (Na metal), a separator (Whatman GF/F glass fiber), and an electrolyte (1 mol $NaPF_6$ in a solution of ethylene carbonate (EC), dimethyl carbonate (DMC), and fluoroethylene carbonate (FEC) in a volume ratio of 49 : 49: 2). The coin cells were assembled in an Ar-filled glove box.

Galvanostatic charge/discharge tests were performed at various C-rates (C/10, C/5, C/2, 1C, 2C, and 5C between 1.7 and 4.2 V) using a battery test system (WonATech WBCS3000). 1C corresponds to ~133 mA g^{-1}.

2.4. Computational details

All the density functional theory (DFT) calculations were performed using the Vienna Ab initio Simulation Package (VASP) [32]. We used projector-augmented wave (PAW) pseudopotentials [33] with a plane-wave basis set as implemented in VASP. Perdew−Burke−Ernzerhof (PBE) parametrization of the generalized gradient approximation (GGA) [34] was used for exchange-correlation functional. For DFT calculations, a 3 × 3 × 2 k-point grid was used to calculate a 1 × 1 × 1 supercell structure of M-$Fe_2(SO_4)_3$. The GGA + U method [35] was adopted to address the localization of the d-orbital in Fe ions, with a U value of 4.2 eV, which was used in the study on the rhombohedral $Fe_2(SO4)_3$ [29]. An appropriate number of k-points and a kinetic energy cutoff of 500 eV are used in all calculations. All structures are optimized until the force in the unit cell converges within 0.02 eV $Å^{-1}$.

NEB calculations [36] were performed to determine the activation barrier for Na diffusion in the M-$Fe_2(SO_4)_3$ structure. A 1 × 2 × 1 supercell is adapted to avoid the interactions between periodic unit cells. To perform the calculations, five intermediate images are generated between each Na site. These structures are then calculated by NEB algorithm with the fixed lattice parameters and free internal atomic positions.

3. Result and discussion

M-$Fe_2(SO_4)_3$ was successfully synthesized by low-temperature heat treatment to prevent thermal decomposition above ~400 °C, such as the formation of other $(SO_4)^{2-}$-based compounds. The detailed experiment process is described in the Experimental section. Scanning electron microscopy (SEM) analysis revealed that the average particle size of M-$Fe_2(SO_4)_3$ ranged between 200 and 600 nm (Supporting Fig. S1). X-ray diffraction (XRD) analysis indicated that the resulting crystal structure of $Fe_2(SO_4)_3$ was a monoclinic structure with a space group of $P\,1\,2_1/n\,1$ without any impurities (Fig. 1a). The overall structure of M-$Fe_2(SO_4)_3$ was investigated through Rietveld refinement based on the XRD pattern. The lattice parameters of M-$Fe_2(SO_4)_3$ were calculated to be a = 8.29422 (11) Å, b = 8.53094(11) Å, and c = 11.62228(15) Å, which are similar to the values reported in literature [25–27]. Other detailed structural information on M-$Fe_2(SO_4)_3$, such as the atomic position, thermal factor and occupancy, is tabulated in Supporting Table T1. In addition, the low values of the reliability factors (R_P = 3.56%, R_I = 2.3%, R_F = 1.66%, χ^2 = 1.69%) indicate the high accuracy of the Rietveld refinement for M-$Fe_2(SO_4)_3$. The crystal structure of M-$Fe_2(SO_4)_3$ based on the Rietveld

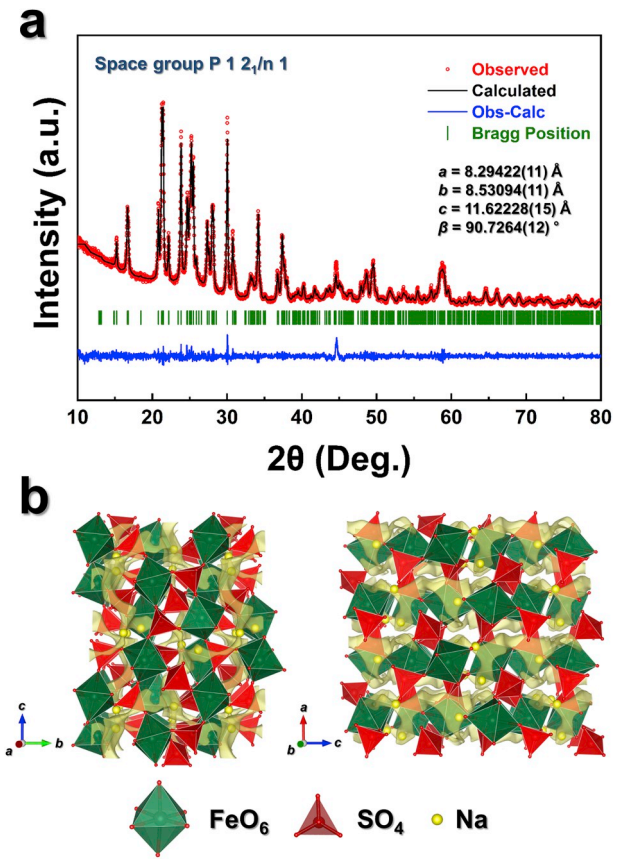

Fig. 1. (a) Rietveld refinement of XRD pattern of M-$Fe_2(SO_4)_3$. (b) BVS energy map of M-$Fe_2(SO_4)_3$ with all possible Na ion sites in the crystal structure.

refinement data is presented in Fig. 1b. Each FeO_6 octahedral is surrounded by six SO_4 tetrahedra through point-sharing of each oxygen ion. The existence of 2 mol Fe^{3+} ions in M-$Fe_2(SO_4)_3$ indicates that ~2 mol Na^+ ions can theoretically be intercalated into the structure via the Fe^{3+}/Fe^{2+} redox reaction, as previously reported for other Fe-based electrode materials [28,29]. In addition, the possible Na^+ ionic sites and diffusion pathways in the M-$Fe_2(SO_4)_3$ structure were verified through the bond-valance sum (BVS) energy map using the Bond_Str program in the FullProf package [37,38]. For the BVS energy map analyses, the atomic position was assumed to be affected by the difference in charge valence of each ion and the type of element. It was predicted that the open crystal structure of M-$Fe_2(SO_4)_3$ with sufficient space may enable facile Na^+ ionic diffusion along three-dimensional paths through Fe^{3+}/Fe^{2+} redox reaction, which implies the outstanding power-capability of M-$Fe_2(SO_4)_3$ as a cathode material for NIBs.

The electrochemical performances of M-$Fe_2(SO_4)_3$ for Na storage were evaluated with Na metal as the reference and counter electrodes using 0.5 M $NaPF_6$ in a 98 : 2 mixture of propylene carbonate (PC) and fluoroethylene carbonate (FEC) as the electrolyte. Fig. 2a presents the charge/discharge profiles and dQ/dV profile of M-$Na_xFe_2(SO_4)_3$ measured at C/10 (1C = ~133 mA g^{-1}) for the voltage range of 1.7–4.2 V (vs. Na^+/Na), which indicates that the average redox potential of M-$Na_xFe_2(SO_4)_3$ is ~3.25 V. Furthermore, M-$Fe_2(SO_4)_3$ delivered a high specific capacity of ~120.3 mAh g^{-1}, corresponding to reversible de/intercalation of ~1.8 mol Na^+ ions, which is larger than that of other Fe- and phosphate-based cathode materials for NIBs [39–41]. The presence of ~1.8 mol Na^+ ions in M-$Fe_2(SO_4)_3$ was verified by inductively coupled plasma (ICP) analyses (Supporting Table T2). Moreover, as shown in Fig. 2b, the presence of Na in M-$Fe_2(SO_4)_3$ further confirmed by transmission electron microscopy (TEM) analyses with elemental mappings obtained using energy-dispersive X-ray spectroscopy (EDS).

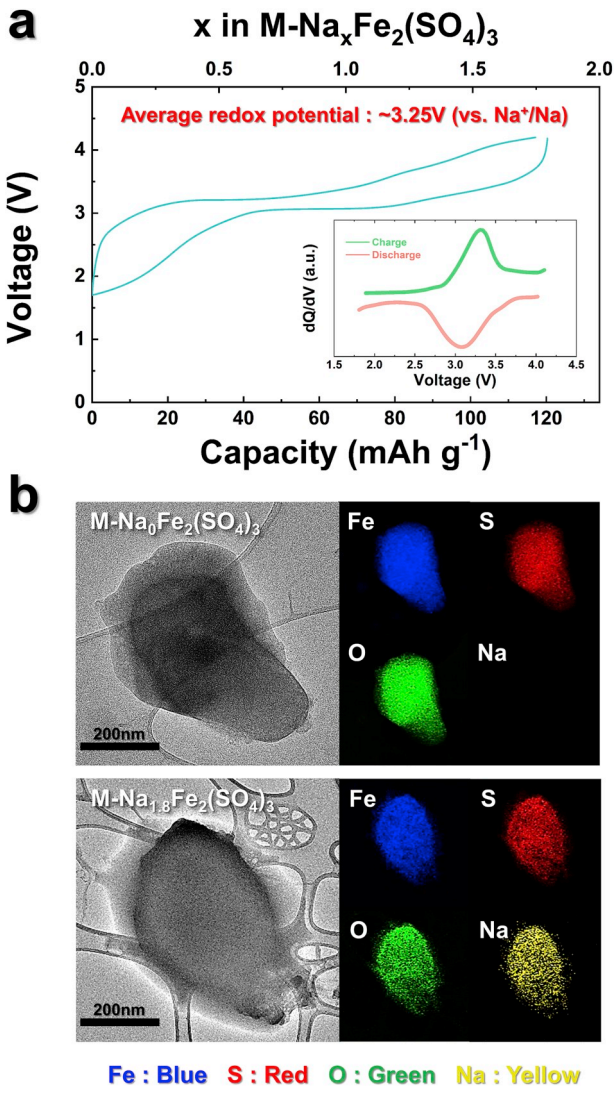

Fig. 2. (a) Charge/discharge profile of M-$Fe_2(SO_4)_3$ in the range of 1.7–4.2 V at C/10. (b) TEM images and EDS elemental mappings for M-$Na_0Fe_2(SO_4)_3$ and M-$Na_{1.8}Fe_2(SO_4)_3$.

The power capability of M-$Fe_2(SO_4)_3$ was verified by comparison of the discharge capacity measured at various currents ranging from C/10 to 5C. As shown in Fig. 3a and b, at a rate of 5C, up to ~76% of the discharge capacity of M-$Na_{1.8}Fe_2(SO_4)_3$ at C/10 was maintained. To understand the underlying reasons for the excellent power capability of M-$Fe_2(SO_4)_3$, we calculated the theoretical activation barrier energy for Na^+ ionic diffusion in the structure using the nudged elastic band (NEB) method based on first-principles calculation. As shown in Fig. 4a, a low activation barrier energy (E_a) of ~505 meV was predicted to be required for Na^+ ionic diffusion along the $Na_{1\text{-}1}$–$Na_{2\text{-}1}$ pathway. Furthermore, the partial Na^+ ions were predicted to only require a very low activation barrier of ~231 meV for Na^+ diffusion along the $Na_{1\text{-}2}$-$Na_{2\text{-}2}$ pathway (Fig. 4b), which is comparable with that for conventional layered-type cathode materials for LIBs [42]. The calculated activation barrier for Na diffusion in the M-$Fe_2(SO_4)_3$ structure was sufficiently low to ensure the facile migration of Na ions along well-interconnected three-dimensional pathways. In addition, it was supposed that smaller difference between the capacity at 2C and that at 5C than the other cases might result from difficulty of 2 mol Na intercalation into the M-$Fe_2(SO_4)_3$. Although 2 mol Na ions can be theoretically intercalated into the M-$Fe_2(SO_4)_3$ structure due to existence of 2 mol Fe^{3+} ions, only ~1.8 mol Na ions could be actually intercalated into the M-$Fe_2(SO_4)_3$,

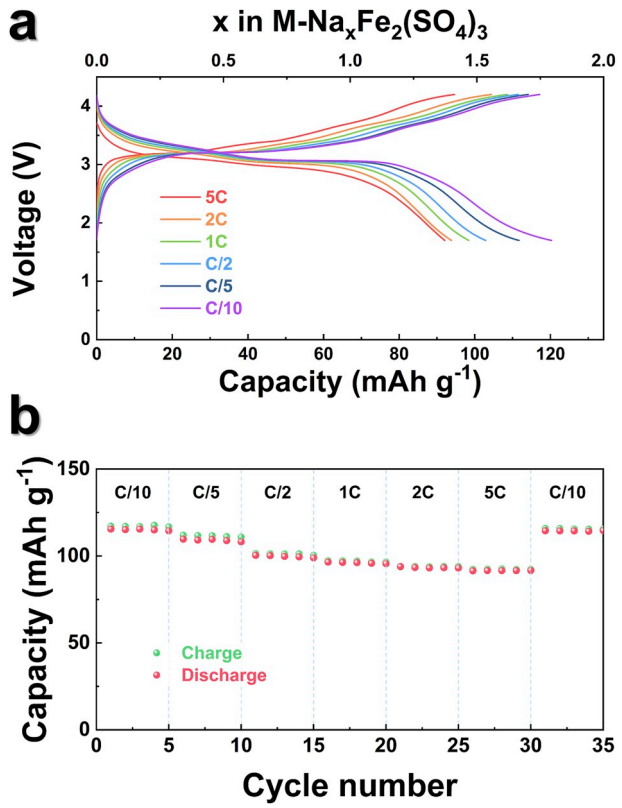

Fig. 3. (a) Charge/discharge profiles of M-$Fe_2(SO_4)_3$ in the range of 1.7–4.2 V at various C-rates. (b) Power-capability of M-$Fe_2(SO_4)_3$.

which implies that despite facile Na diffusion into the structure, further Na intercalation may be hard after intercalating the certain amounts of Na ions into the M-$Fe_2(SO_4)_3$ structure. Thus, because the capacities measured at 2C and at 5C are relatively smaller than the capacities measured at the low current rates and facile Na diffusion is possible in the structure, the M-$Fe_2(SO_4)_3$ electrode may experience relatively weak capacity fading from 2C to 5C compared with that from C/10 to C/5.

Furthermore, at 1C, M-$Fe_2(SO_4)_3$ exhibited a capacity retention of ~78% compared with the initial capacity over 1000 cycles, with a high coulombic efficiency of over 99% (Fig. 5a). The unexpectedly outstanding cycle performance of M-$Fe_2(SO_4)_3$ is thought to be related to the small volume change during the charging/discharging process. In addition, we supposed that despite the small volume expansion, the side-reactions might result in capacity loss of the Na-cell consisting of M-$Fe_2(SO_4)_3$ during repeated charge/discharge. It is known that decrease of the capacity after the long cycle test may result from irreversible side reactions, such as decomposition of electrolytes, exfoliation of electrode from current collector, structural degradation of electrode materials, *etc* [43–46]. As shown in Supporting Fig. S2, it was verified that with increasing the number of charge/discharge, polarization effect on the charge/discharge curve of M-$Fe_2(SO_4)_3$ got larger, which implies the resistance-increase of the Na-cell consisting of M-$Fe_2(SO_4)_3$ by the side-reactions occurred during charge/discharge, such as the electrolyte-decomposition, *etc*. To understand the outstanding electrochemical properties, we prepared various M-$Na_xFe_2(SO_4)_3$ ($0 \le x \le 1.8$) samples with different Na contents for *ex situ* XRD analyses (Supporting Fig. S3); the Na content of each sample was determined by controlling the charged state. No contaminations or severe structural degradation was detected in any of the *ex situ* XRD patterns of M-$Na_xFe_2(SO_4)_3$. The intensities of partial XRD peaks, such as (111), (020), (210), (220) and (004), continuously changed during discharging process (Fig. 5b), which indicates the occurrence of a structural change of M-$Na_xFe_2(SO_4)_3$

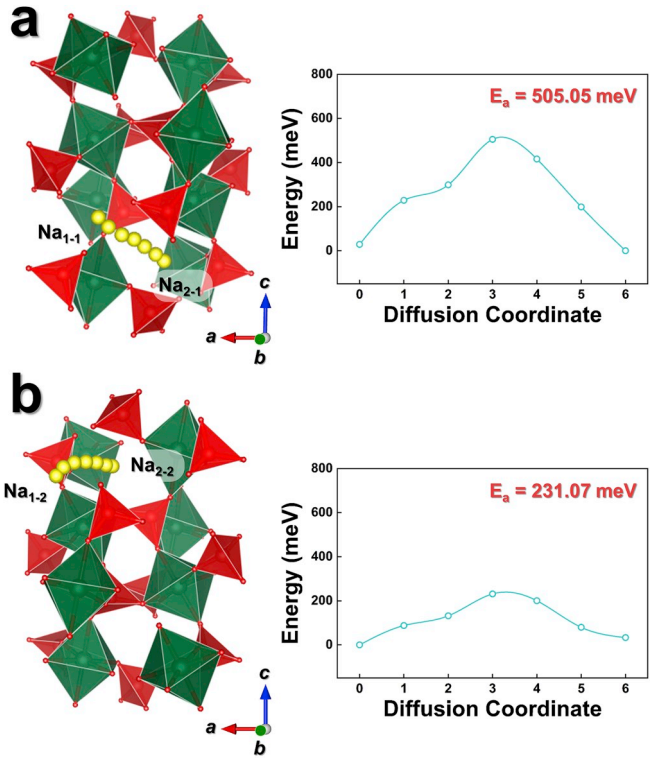

Fig. 4. (a) $Na_{1\text{-}1}$–$Na_{2\text{-}1}$ and (b) $Na_{1\text{-}2}$–$Na_{2\text{-}2}$ diffusion pathways and their energy landscapes determined NEB method.

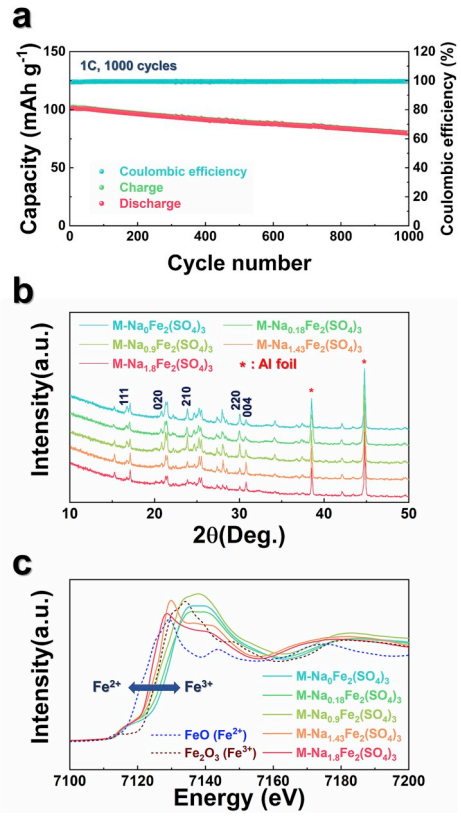

Fig. 5. (a) Cycle performance of M-$Fe_2(SO_4)_3$ at 1C over 1000 cycles. (b) *Ex situ* XRD patterns of M-$Na_xFe_2(SO_4)_3$ ($0 \le x \le 1.8$). (c) Fe K-edge XANES spectra of M-$Na_xFe_2(SO_4)_3$ ($0 \le x \le 1.8$).

resulting from the intercalation of Na^+ ions into the structure. Furthermore, X-ray absorption near-edge structure (XANES) analyses verified that the Fe oxidation state of M-$Na_xFe_2(SO_4)_3$ was significantly affected by the Na content in the structure. As observed in Fig. 5c, the Fe K-edge was shifted toward a lower energy level during the discharging process, which indicates that the Fe^{3+}/Fe^{2+} redox reaction of M-Na_x-$Fe_2(SO_4)_3$ was accompanied by Na^+ de/intercalation.

Interestingly, numerous Na ions were de/intercalated from/into the structure, which implies that the volume and lattice parameter changes for M-$Na_xFe_2(SO_4)_3$ were negligible during the charging/discharging process. Fig. 6 shows that the total volume difference between the M-$Na_0Fe_2(SO_4)_3$ and M-$Na_{1.8}Fe_2(SO_4)_3$ structures was just ~1%. It is likely that the slight volume change of M-$Na_{1.8}Fe_2(SO_4)_3$ during charging/discharging can be attributed to its structural stability supported by the presence of covalent $(SO_4)^{2-}$ polyanion in the crystal structure, which differs from the large volume changes of general layered-type cathode materials for NIBs resulting from O^{2-}–O^{2-} repulsion during the Na^+ de/intercalation process [47–49]. Furthermore, the open structure of M-$Fe_2(SO_4)_3$ may be another reason for its small volume change, as it may provide the sufficient space for the displacement of ions in the structure without severe volume expansion or shrinkage [50].

Additionally, we compared the morphology and *ex situ* XRD patterns of the pristine M-$Fe_2(SO_4)_3$ electrode with those of the electrode after 1000 cycles (Supporting Fig. S4). Because of the negligible volume difference between M-$Na_0Fe_0(SO_4)_3$ and M-$Na_{1.8}Fe_2(SO_4)_3$, the morphology of M-$Fe_2(SO_4)_3$ after 1000 cycles was well retained without severe cracking or structural degradation despite the long-term cycling, as reflected by the lack of degradation of the crystal structure in the XRD pattern after 1000 cycles. Thus, it is supposed that the small volume change of M-$Fe_2(SO_4)_3$ during charging/discharging may result in the exceptionally outstanding cycle performance of M-$Fe_2(SO_4)_3$ as a promising cathode for NIBs. Furthermore, based on the experimental results, we prepared a Ragone plot to compare the electrochemical characteristics of previously reported Fe-based cathode materials with those of M-$Fe_2(SO_4)_3$. In Supporting Fig. S5, it is confirmed that M-$Fe_2(SO_4)_3$ exhibits better electrochemical performances than other pristine Fe-based polyanion materials [30,51–53]. These remarkable performances of M-$Fe_2(SO_4)_3$ may be attributed to the low activation barrier energy in diffusion process as well as the small volume expansion during Na^+ de/intercalation.

4. Conclusion

In summary, we prepared the M-$Fe_2(SO_4)_3$ as a novel cathode material for NIBs using a low-temperature synthesis process. Using XRD analyses with Rietveld refinement, we obtained structural information on the M-$Fe_2(SO_4)_3$, including the lattice parameters and atomic positions. A theoretical approach using BVS energy map revealed the possibility of not only Na^+ intercalation into the M-$Fe_2(SO_4)_3$ structure but also Na^+ ionic diffusion along three-dimensional pathways. During the Na^+ de/intercalation process at C/10 (1C = ~133 mA g^{-1}), M-$Fe_2(SO_4)_3$ exhibited a large specific capacity of ~120.3 mAh g^{-1}, corresponding to ~1.8 mol Na^+ ions with a high average operation voltage of ~3.25 V (*vs.* Na^+/Na). Furthermore, even at 5C, up to 76% of the discharge capacity of M-$Fe_2(SO_4)_3$ at C/10 was maintained, indicating its excellent power capability. The low activation barrier energy of M-$Fe_2(SO_4)_3$ for Na^+ ionic diffusion was verified using the NEB method based on first-principles calculations, which supports the outstanding power capability of M-$Fe_2(SO_4)_3$. In particular, M-$Fe_2(SO_4)_3$ exhibited exceptionally outstanding cycle performance with retention of ~78% of the initial capacity over 1000 cycles at a current rate of 1C, which is attributed to its small volume change (~1%) during the Na^+ de/intercalation process. We believe that our findings on M-$Fe_2(SO_4)_3$ will be beneficial for the development of new electrode materials with high energy density for not only NIBs but also different types of rechargeable batteries.

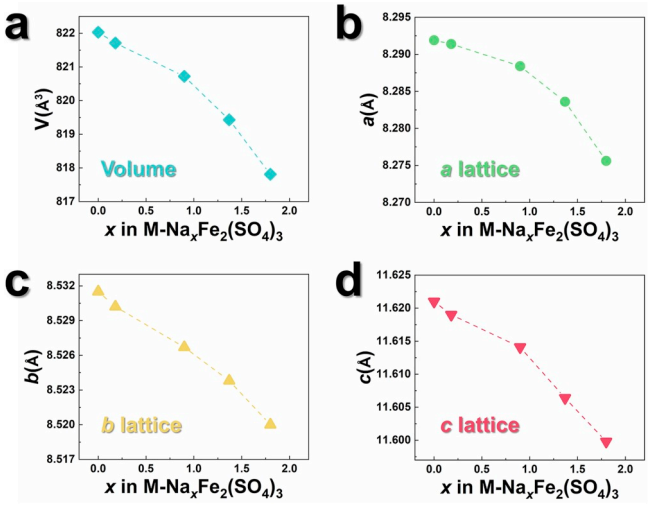

Fig. 6. Changes in (a) volume, (b) lattice parameter *a*, (c) lattice parameter *b*, and (d) lattice parameter *c* of M-$Na_xFe_2(SO_4)_3$ ($0 \leq x \leq 1.8$) as a function of Na content.

Conflicts of interest

There are no conflicts to declare.

Acknowledgements

This work was supported by the Research Fund (PNK6080) of the Korea Institute of Materials Science (KIMS) of the Republic of Korea. This work was also supported by the National Research Foundation of Korea funded by the Ministry of Science & ICT of the Republic of Korea (NRF-2019R1F1A1063415).

Appendix A. Supplementary data

Supplementary data to this article can be found online at https://doi.org/10.1016/j.jpowsour.2019.226750.

References

[1] S.F. Tie, C.W. Tan, A review of energy sources and energy management system in electric vehicles, Renew. Sustain. Energy Rev. 20 (2013) 82–102, https://doi.org/10.1016/j.rser.2012.11.077.
[2] B. Dunn, H. Kamath, J.-M. Tarascon, Electrical energy storage for the grid: a battery of choices, Science 334 (2011) 928–935, https://doi.org/10.1126/science.1212741.
[3] J.B. Goodenough, Electrochemical energy storage in a sustainable modern society, Energy Environ. Sci. 7 (2014) 14–18, https://doi.org/10.1039/C3EE42613K.
[4] G. Jeong, Y.-U. Kim, H. Kim, Y.-J. Kim, H.-J. Sohn, Prospective materials and applications for Li secondary batteries, Energy Environ. Sci. 4 (2011) 1986, https://doi.org/10.1039/c0ee00831a.
[5] A. Konarov, S.-T. Myung, Y.-K. Sun, Cathode materials for future electric vehicles and energy storage systems, ACS Energy Lett 2 (2017) 703–708, https://doi.org/10.1021/acsenergylett.7b00130.
[6] Z. Wang, L. Zhou, X.W. Lou, Metal oxide hollow nanostructures for lithium-ion batteries, Adv. Mater. 24 (2012) 1903–1911, https://doi.org/10.1002/adma.201200469.
[7] V. Etacheri, R. Marom, R. Elazari, G. Salitra, D. Aurbach, Challenges in the development of advanced Li-ion batteries: a review, Energy Environ. Sci. 4 (2011) 3243, https://doi.org/10.1039/c1ee01598b.
[8] B. Scrosati, J. Garche, Lithium batteries: status, prospects and future, J. Power Sources 195 (2010) 2419–2430, https://doi.org/10.1016/J.JPOWSOUR.2009.11.048.
[9] N. Nitta, F. Wu, J.T. Lee, G. Yushin, Li-ion battery materials: present and future, Mater. Today 18 (2015) 252–264, https://doi.org/10.1016/j.mattod.2014.10.040.
[10] S.W. Kim, D.H. Seo, X. Ma, G. Ceder, K. Kang, Electrode materials for rechargeable sodium-ion batteries: potential alternatives to current lithium-ion batteries, Adv. Energy Mater. 2 (2012) 710–721, https://doi.org/10.1002/aenm.201200026.
[11] L. Wang, Y. Lu, J. Liu, M. Xu, J. Cheng, D. Zhang, J.B. Goodenough, A superior low-cost cathode for a Na-ion battery, Angew. Chem. Int. Ed. 52 (2013) 1964–1967, https://doi.org/10.1002/anie.201206854.

[12] S.Y. Hong, Y. Kim, Y. Park, A. Choi, N.-S. Choi, K.T. Lee, Charge carriers in rechargeable batteries: Na ions *vs.* Li ions, Energy Environ. Sci. 6 (2013) 2067, https://doi.org/10.1039/c3ee40811f.

[13] V. Palomares, P. Serras, I. Villaluenga, K.B. Hueso, J. Carretero-González, T. Rojo, Na-ion batteries, recent advances and present challenges to become low cost energy storage systems, Energy Environ. Sci. 5 (2012) 5884, https://doi.org/10.1039/c2ee02781j.

[14] B.L. Ellis, L.F. Nazar, Sodium and sodium-ion energy storage batteries, Curr. Opin. Solid State Mater. Sci. 16 (2012) 168–177, https://doi.org/10.1016/J.COSSMS.2012.04.002.

[15] N. Yabuuchi, K. Kubota, M. Dahbi, S. Komaba, Research development on sodium-ion batteries, Chem. Rev. 114 (2014) 11636–11682, https://doi.org/10.1021/cr500192f.

[16] J.-Y. Hwang, S.-T. Myung, Y.-K. Sun, Sodium-ion batteries: present and future, Chem. Soc. Rev. 46 (2017) 3529–3614, https://doi.org/10.1039/C6CS00776G.

[17] H. Hou, C.E. Banks, M. Jing, Y. Zhang, X. Ji, Carbon quantum dots and their derivative 3D porous carbon frameworks for sodium-ion batteries with ultralong cycle life, Adv. Mater. 27 (2015) 7861–7866, https://doi.org/10.1002/adma.201503816.

[18] A. Manthiram, J.B. Goodenough, Lithium insertion into $Fe_2(SO_4)_3$ frameworks, J. Power Sources 26 (1989) 403–408, https://doi.org/10.1016/0378-7753(89)80153-3.

[19] S. Okada, Y. JI, Iron-based cathodes/anodes for Li-ion and post Li-ion batteries, J. Ind. Eng. Chem. 10 (2004) 1104–1113. https://www.cheric.org/research/tech/periodicals/view.php?seq=458601.

[20] M. Reynaud, M. Ati, B.C. Melot, M.T. Sougrati, G. Rousse, J.-N. Chotard, J.-M. Tarascon, $Li_2Fe(SO_4)_2$ as a 3.83 V positive electrode material, Electrochem, Commun. Now. 21 (2012) 77–80, https://doi.org/10.1016/J.ELECOM.2012.04.027.

[21] D. Dwibedi, C.D. Ling, R.B. Araujo, S. Chakraborty, S. Duraisamy, N. Munichandraiah, R. Ahuja, P. Barpanda, Ionothermal synthesis of high-voltage alluaudite $Na_{2+2x}Fe_{2-x}(SO_4)_3$ sodium insertion compound: structural, electronic, and magnetic insights, ACS Appl. Mater. Interfaces 8 (2016) 6982–6991, https://doi.org/10.1021/acsami.5b11302.

[22] G.J. Long, G. Longworth, P. Battle, A.K. Cheetham, R.V. Thundathil, D. Beveridge, A study of anhydrous iron(III) sulfate by magnetic susceptibility, Moessbauer, and neutron diffraction techniques, Inorg. Chem. 18 (1979) 624–632, https://doi.org/10.1021/ic50193a021.

[23] F. Wang, N. Zhang, X. Zhao, L. Wang, J. Zhang, T. Wang, F. Liu, Y. Liu, L. Fan, Realizing a high-performance Na-storage cathode by tailoring ultrasmall Na_2FePO_4F nanoparticles with facilitated reaction kinetics, Adv. Sci. (2019), 1900649, https://doi.org/10.1002/advs.201900649.

[24] K.S. Nanjundaswamy, A.K. Padhi, J.B. Goodenough, S. Okada, H. Ohtsuka, H. Arai, J. Yamaki, Synthesis, redox potential evaluation and electrochemical characteristics of NASICON-related-3D framework compounds, Solid State Ionics 92 (1996) 1–10, https://doi.org/10.1016/S0167-2738(96)00472-9.

[25] J. Majzlan, A. Navrotsky, R. Stevens, M. Donaldson, B.F. Woodfield, J. Boerio-Goates, Thermodynamics of monoclinic $Fe_2(SO_4)_3$, J. Chem. Thermodyn. 37 (2005) 802–809, https://doi.org/10.1016/j.jct.2004.11.021.

[26] P.C. Christidis, P.J. Rentzeperis, The crystal structure of the monoclinic $Fe_2(SO_4)_3$, Zeitschrift Für Krist. 141 (1975) 233–245, https://doi.org/10.1524/zkri.1975.141.3-4.233.

[27] P.C. Christidis, P.J. Rentzeperis, A. Kirfel, G. Will, X-ray determination of the electron density distribution in monoclinic $Fe_2(SO_4)_3$, Z. für Kristallogr. - Cryst. Mater. 164 (1983) 219–236, https://doi.org/10.1524/zkri.1983.164.3-4.219.

[28] D. Dwibedi, P. Barpanda, Solution-assisted energy-savvy synthesis of high-voltage $Na_2M_2(SO_4)_3$ (M = 3d metals) alluaudite family of sodium insertion materials, Mater. Today Proc. 5 (2018) 23439–23442, https://doi.org/10.1016/j.matpr.2018.11.085.

[29] S.-C. Chung, J. Ming, L. Lander, J. Lu, A. Yamada, Rhombohedral NASICON-type $Na_xFe_2(SO_4)_3$ for sodium-ion battery: comparison with the phosphate and alluaudite phases, J. Mater. Chem. A. 6 (2018) 3919–3925, https://doi.org/10.1039/C7TA08606G.

[30] C.W. Mason, I. Gocheva, H.E. Hoster, D.Y.W. Yu, Iron(III) sulfate: a stable, cost effective electrode material for sodium ion batteries, Chem. Commun. 50 (2014) 2249–2251, https://doi.org/10.1039/C3CC47557C.

[31] P. Barpanda, G. Oyama, S. Nishimura, S.-C. Chung, A. Yamada, A 3.8-V earth-abundant sodium battery electrode, Nat. Commun. 5 (2014) 4358, https://doi.org/10.1038/ncomms5358.

[32] G. Kresse, J. Furthmüller, Efficiency of ab-initio total energy calculations for metals and semiconductors using a plane-wave basis set, Comput. Mater. Sci. 6 (1996) 15–50, https://doi.org/10.1016/0927-0256(96)00008-0.

[33] P.E. Blöchl, Projector augmented-wave method, Phys. Rev. B 50 (1994) 17953–17979, https://doi.org/10.1103/PhysRevB.50.17953.

[34] J.P. Perdew, K. Burke, M. Ernzerhof, Generalized gradient approximation made simple, Phys. Rev. Lett. 77 (1996) 3865–3868, https://doi.org/10.1103/PhysRevLett.77.3865.

[35] V.I. Anisimov, F. Aryasetiawan, A.I. Lichtenstein, First-principles calculations of the electronic structure and spectra of strongly correlated systems: the LDA + U method, J. Phys. Condens. Matter 9 (1997) 767–808, https://doi.org/10.1088/0953-8984/9/4/002.

[36] G. Henkelman, B.P. Uberuaga, H. Jónsson, A climbing image nudged elastic band method for finding saddle points and minimum energy paths, J. Chem. Phys. 113 (2000) 9901–9904, https://doi.org/10.1063/1.1329672.

[37] J. Rodríguez-Carvajal, Recent developments of the program FULLPROF, Comm. Powder Diffr. (IUCr). Newsl. 26 (2001) 12–19.

[38] S. Adams, Modelling ion conduction pathways by bond valence pseudopotential maps, Solid State Ionics 136–137 (2000) 1351–1361, https://doi.org/10.1016/S0167-2738(00)00576-2.

[39] H. Kim, R.A. Shakoor, C. Park, S.Y. Lim, J.-S. Kim, Y.N. Jo, W. Cho, K. Miyasaka, R. Kahraman, Y. Jung, J.W. Choi, $Na_2FeP_2O_7$ as a promising iron-based pyrophosphate cathode for sodium rechargeable batteries: a combined experimental and theoretical study, Adv. Funct. Mater. 23 (2013) 1147–1155, https://doi.org/10.1002/adfm.201201589.

[40] J. Lu, S. Nishimura, A. Yamada, A Fe-rich sodium iron orthophosphate as cathode material for rechargeable batteries, Electrochem. Commun. 79 (2017) 51–54, https://doi.org/10.1016/j.elecom.2017.04.012.

[41] P. Barpanda, G. Liu, C.D. Ling, M. Tamaru, M. Avdeev, S.C. Chung, Y. Yamada, A. Yamada, $Na_2FeP_2O_7$: a safe cathode for rechargeable sodium-ion batteries, Chem. Mater. 25 (2013) 3480–3487, https://doi.org/10.1021/cm401657c.

[42] F. Ning, S. Li, B. Xu, C. Ouyang, Strain tuned Li diffusion in $LiCoO_2$ material for Li ion batteries: a first principles study, Solid State Ionics 263 (2014) 46–48, https://doi.org/10.1016/j.ssi.2014.05.008.

[43] Y.-U. Park, D.-H. Seo, H.-S. Kwon, B. Kim, J. Kim, H. Kim, I. Kim, H.-I. Yoo, K. Kang, A new high-energy cathode for a Na-ion battery with ultrahigh stability, J. Am. Chem. Soc. 135 (2013) 13870–13878, https://doi.org/10.1021/ja406016j.

[44] C.-H. Jo, J.U. Choi, H. Yashiro, S.-T. Myung, Controllable charge capacity using a black additive for high-energy-density sodium-ion batteries, J. Mater. Chem. A. 7 (2019) 3903–3909, https://doi.org/10.1039/C8TA09833F.

[45] J. Kim, G. Yoon, H. Kim, Y.-U. Park, K. Kang, $Na_3V(PO_4)_2$: a new layered-type cathode material with high water stability and power capability for Na-ion batteries, Chem. Mater. 30 (2018) 3683–3689, https://doi.org/10.1021/acs.chemmater.8b00458.

[46] M.K. Cho, J.H. Jo, J.U. Choi, J. Kim, H. Yashiro, S. Yuan, L. Shi, Y.-K. Sun, S.-T. Myung, Tunnel-type β-FeOOH cathode material for high rate sodium storage via a new conversion reaction, Nano Energy 41 (2017) 687–696, https://doi.org/10.1016/J.NANOEN.2017.10.022.

[47] H. Yoshida, N. Yabuuchi, S. Komaba, $NaFe_{0.5}Co_{0.5}O_2$ as high energy and power positive electrode for Na-ion batteries, Electrochem. Commun. 34 (2013) 60–63, https://doi.org/10.1016/j.elecom.2013.05.012.

[48] S.-M. Oh, S.-T. Myung, J.-Y. Hwang, B. Scrosati, K. Amine, Y.-K. Sun, High capacity O3-type $Na[Li_{0.05}(Ni_{0.25}Fe_{0.25}Mn_{0.5})_{0.95}]O_2$ cathode for sodium ion batteries, Chem. Mater. 26 (2014) 6165–6171, https://doi.org/10.1021/cm502481b.

[49] J.U. Choi, C.S. Yoon, Q. Zhang, P. Kaghazchi, Y.H. Jung, K.-S. Lee, D.-C. Ahn, Y.-K. Sun, S.-T. Myung, Understanding on the structural and electrochemical performance of orthorhombic sodium manganese oxides, J. Mater. Chem. A. 7 (2019) 202–211, https://doi.org/10.1039/C8TA08796B.

[50] J. Kim, G. Yoon, M.H. Lee, H. Kim, S. Lee, K. Kang, New 4V-class and zero-strain cathode material for Na-ion batteries, Chem. Mater. 29 (2017) 7826–7832, https://doi.org/10.1021/acs.chemmater.7b02477.

[51] Y. Fang, Q. Liu, L. Xiao, X. Ai, H. Yang, Y. Cao, High-Performance Olivine $NaFePO_4$ Microsphere Cathode Synthesized by Aqueous Electrochemical Displacement Method for Sodium Ion Batteries, 2015, https://doi.org/10.1021/acsami.5b04691.

[52] J.S. Ko, V.V.T. Doan-Nguyen, H.-S. Kim, X. Petrissans, R.H. Deblock, C.S. Choi, J. W. Long, B.S. Dunn, High-rate Capability of Na_2FePO_4F Nanoparticles by Enhancing Surface Carbon Functionality for Na-Ion Batteries, 2017, https://doi.org/10.1039/c7ta05680j.

[53] P. Singh, K. Shiva, H. Celio, J.B. Goodenough, Eldfellite, $NaFe(SO_4)_2$: an intercalation cathode host for low-cost Na-ion batteries, Energy Environ. Sci. 8 (2015) 3000–3005, https://doi.org/10.1039/C5EE02274F.